Journal of Engineering Mathematics **40:** 141–158, 2001.

Mathematical modelling of long ocean waves with a discontinuous density gradient

A. OUAHSINE and P. A. BOIS
Laboratoire de Mécanique de Lille, U.R.A. CNRS 1441, F-59655 Villeneuve d'Ascq, France
e-mail: ouahsine@univ-lille1.fr

Received 6 January 1999; accepted in revised form 17 May 2000

Abstract. A mathematical model for studying the propagation of long internal ocean waves of finite amplitude is proposed. The vertical structure of the pressure perturbation is investigated and reduced to a Sturm–Liouville eigenvalue problem. In the continuous stratification case, the pattern of this vertical structure depends on the choice of the characteristic scale of a varying stratification parameter, denoted by δ. As this parameter asymptotically approaches a critical value (*i.e.* $\delta \to \delta_{\text{cri}}$), the amplitudes of the solution's normal modes increase considerably. The internal waves break and produce an unstable interface, which degenerates into a turbulent mixed layer. These conditions correspond to the critical state of wave existence. When $\delta < \delta_{\text{cri}}$ a three-layer discontinuous gradient model is proposed to resolve the problem. It consists in specifying one solution within a thin intermediary layer and two solutions on either side of this layer. The results show that the use of appropriately matching interfacial conditions allows to obtain generally matching solutions, even for small values of the nonconstant stratification parameter δ.

Key words: long waves, stratification, frontogenesis, density gradient, matched asymptotics

1. Introduction

This paper is concerned with waves propagating in density-stratified fluids with a thin density interface. The presence of such an interface continues to be a perplexing problem in environmental and geophysical fluid dynamics. Since the interfacial layer is thin, the waves can be limited in their spectral density by sporadic local instabilities, and when the waves break, they produce turbulence [1]. This process produces a turbulent mixing between fluids of different density, leading to the overturning waves by static instability. The instability process is initially described here as one involving homogeneous density distributions on either side of the turbulent region. When an appreciable density difference between the turbulent and non-turbulent regions develops, new effects become discernible. A thin pycnocline or thermocline develops, in which the ambient fluid is initially statically stable (*i.e.* $\partial\rho_0/\partial z < 0$). However, if there is sufficient shear or wave energy coming from the breaking of large amplitude internal-waves, dynamical instability can give rise to vortical formations (rolls or billows). In this study we use a linear analysis to derive the growth rate of the finite-amplitude waves. The instability is interpreted as a criterion in which the waves grow, in inverse proportion to the parameter of varying stratification δ, until they attain their maximum amplitudes and break. When the breaking mechanism occurs, a linear analysis is no longer valid and a nonlinear analysis is required to consider the effects of low-frequency waves. However, the breaking mechanism in itself is not within the scope of this study.

When a density gradient exists in a fluid that complies with the Boussinesq approximation [2], vorticity may be generated and flow is induced. The resulting motion advects fluid particles and the density gradient may either decrease or increase. In the latter case, the density gradient may increase to such an extent that an effective discontinuity or a front may develop [1, 3]. In stratified fluids fronts are regions where mixing occurs [4–6], and once frontogenesis has occurred, flow characteristics undergo a fundamental change. The Kelvin-Helmholtz billowing mechanism and the breaking of internal waves are some of the different forms of motion that may characterize this change [1–8].

Several attempts have been made to investigate internal waves in terms of thickness of the interfacial layer. Davis and Acrivos [9] examined experimentally the case of a small quantity of neutrally buoyant fluid being slowly injected into a thin interfacial region between two fluids of different densities. Two types of waves were observed: first, small-amplitude waves characterized by open streamlines and propagating with only gradual amplitude attenuation; and second, large-amplitude waves characterized by a region of fluid trapped within closed streamlines. Stamp and Jacka [10] carried out a study of deep-water internal solitary waves propagating in a thin interface between two fluids of different densities. They showed that small waves cause changes in energy and momentum, whereas sufficiently large waves disperse the energy and cause the mixture of fluids. They added that the weakly nonlinear theory fails to account for the behavior of large-amplitude waves, nor does it comply with the criterion requiring waves to maintain permanent form, despite the fact that their wavelength must decrease when their amplitude increases; instead, the wavelength of large waves was observed to grow with increasing amplitude. Pawlak and Armi [11] proposed an experimental and analytical study of the combined effects of buoyancy and acceleration of a stratified shear layer on the dynamics of a mixing layer. They observed a new finite amplitude mechanism in which the core of a newly generated vortex is separated from its source vortex at the interface. A second formation appears and gives rise to a modified and duplicated vortex. The spatial linear stability analysis reveals that one of two modified Kelvin-Helmholtz modes is dominant. The mixing induced by the interface instabilities is such that a strong density gradient occurs in the high-momentum streams, and a low-gradient region occurs when lower-momentum streams are involved.

Internal waves are reported to have fairly large amplitudes, somewhat larger than 100 m, and may generate slowly varying local currents in open ocean or in fjords. Such induced currents are important factors to be considered when determining the dimensions of offshore platforms operating in deep water areas where internal waves might occur. Knowledge about the properties of internal waves and their potential consequences has therefore real-world relevance. Recently, Grue *et al.* [12] have conducted a theoretical and experimental study on the properties of solitary waves propagating in a two-layer fluid. The experiments involved the case where a relatively thin pycnocline layer separates fresh water from salt water. They showed that rolls due to the Kelvin–Helmholtz instability develop and the pycnocline is locally diminished. The theoretical models include a fully nonlinear model and a weakly nonlinear Korteweg–de Vries (KdV) model. Strong agreement between the experiment and the results provided by the fully nonlinear model was observed, except when unstable motion in the pycnocline is involved. The KdV model deviated from the experiments and the fully nonlinear theory, most notably when large amplitude waves were present.

In stratified water and in water in which the density varies with depth, internal waves may occur in different forms with various propagation characteristics. For example, these waves may have the character of small but finite amplitude waves [13], of which the wavelengths are

considerably greater than the total fluid depth. These waves are called shallow-water waves, for which the principal approximations are $\lambda/H \gg 1$ and $h/H = O(1)$, where $2H$ is the total fluid depth and $2h$ is the depth of the stratification. A second example, is provided by waves having the character of long waves [9], but with wavelengths which are much smaller than the total fluid depth but much greater than the depth of the stratification: $h/H \to 1$ and $\lambda/h \gg 1$. In this study, we are interested in this second type of wave in which the density is a continuous function of depth.

In Section 2 we present a mathematical model of long waves propagation in fluids with variable-gradient stratification, derive the mathematical problem and formulate the asymptotic model. In Section 3, different model parameters are defined and analyzed to obtain a set of differential equations of the boundary-value problem. In Section 4, the development of the modal structures for the eigenvalues problem, including a variable-density profile is discussed. Section 5 is devoted to the study of the three-layer discontinuous gradient model.

2. Mathematical formulation of the problem

We consider an incompressible and stratified fluid in a rotating coordinate frame, and we assume that the Boussinesq approximation is valid in order to take into account the density variations. Moreover, the hydrostatic balance is used. The equations describing this motion are available in the literature (Pedlosky [14], Godts [15], Bois *et al.* [16], Ouahsine [17]). The present analysis is valid for long-wave motions, where it has been posited that $\varepsilon = H/L \ll 1$, and where L and H are the horizontal and vertical characteristic scales, respectively. Let $\mathbf{v}$ be the horizontal velocity vector (with eastward and northward component u and v), and let w be the vertical velocity. By focussing on the O (100 km) scales, we can use the mid-latitudes β-plane approximation, which can be formulated as $\delta = L/a_0 \ll 1$, a_0 being the Earth's radius. In what follows, we use a Cartesian frame (x, y, z), where x increases to the East, y to the North and z upwards. Let T_0, U_0, R, Π be the characteristics scales for time t, for the horizontal velocity (u, v), for the density ϱ and for the pressure p, respectively. Consequently, the non-dimensional relations are selected as follows:

$$(X, Y) = (x, y)L, \quad Z = zH, \quad T = tT_0,$$

$$(U, V) = (u, v)U_0, \quad W = wU_0H/L, \quad p = \bar{p}\Pi, \quad \varrho = \bar{\varrho}R.$$

The equations below describe the motion of an incompressible rotating fluid:

$$\begin{aligned} &\varrho\left(\mathrm{Ro}\left(\mathrm{St}\frac{\partial \mathbf{v}}{\partial t} + \mathbf{v}\cdot\mathbf{D}\mathbf{v} + w\frac{\partial \mathbf{v}}{\partial z}\right) + (1 + \mathrm{Ro}\beta y)k \times \mathbf{v}\right) + \frac{\mathrm{Ro}}{\mathrm{Fr}^2}\mathbf{D}p = \mathrm{E_v}\frac{\partial^2 \mathbf{v}}{\partial z^2} + \mathbf{D}^2\mathbf{v}, \\ &\frac{\partial p}{\partial z} + \mathrm{Bo}\,\varrho = 0, \quad \mathbf{D}\cdot\mathbf{v} + \frac{\partial w}{\partial z} = 0, \quad \mathrm{St}\frac{\partial \varrho}{\partial t} + \mathbf{v}\cdot\mathbf{D}\varrho + \mathbf{w}\frac{\partial \rho}{\partial z} = 0. \end{aligned} \tag{1}$$

For simplicity, we dropped the overbars on the variables $\bar{p}$ and $\bar{\varrho}$.

Here (**i, j, k**) are unit vectors oriented eastwards, northwards, and locally upward, $\mathbf{D} = (\partial/\partial x, \partial/\partial y)$, t is the time, p the pressure and $f_0 = 2\Omega \sin\lambda_0$ designates the local Coriolis parameter where λ_0 is the latitude and $\Omega = 7 \cdot 3\ 10^{-3}$ rad/s is the earth's rotation. Further, Ro, Fr, St, Bo are dimensionless numbers defined by:

$\mathrm{Ro} = U_0/f_0L$: the Rossby number; $\mathrm{St} = L/U_0T_0$: the Strouhal number;
$\mathrm{Fr} = U_0/\sqrt{gH}$ the Froude number; $\mathrm{Bo} = RgH/\Pi$: non-dimensional number.

The vertical and horizontal Ekman numbers are respectively:

$$\mathrm{E_v} = \nu/f_0 H^2 \quad \text{and} \quad \mathrm{E_h} = \nu/f_0 L^2.$$

The boundary conditions at the bottom are: $\mathbf{v} = \mathbf{0}$, $w = 0$, and the initial conditions (at $t = 0$) are: $\mathbf{v} = \mathbf{v}^0$, and $p = p_0$, where $\mathbf{v}^0$ and p_0 are known.

To establish the boundary conditions on the sea's surface we assume that, in a state of equilibrium, motion is controlled by surface wind stress $[\tau]_w$. It follows that the kinematic condition of this stress at the ocean-atmosphere interface is specified by [15]:

$$[\tau]_i = [-p\mathbf{n}I_d + 2\mu\mathbf{n}D]_i \quad \text{and} \quad p = p_a, \tag{2}$$

where $\mathbf{n}$ is the unit normal vector of the interface, D is the tensor rate of deformation, I_d is the tensor unit and p_a is the atmospheric pressure. The bracket $[u]_i$ denotes the jump of the function u across the interface i. This last condition on the surface level can be written:

$$\left[\mu \frac{U}{L}\frac{\partial \mathbf{v}}{\partial z}\right]_i = 0 \tag{3}$$

and

$$\left[-p + 2\mu \frac{U}{L}\frac{\partial w}{\partial z}\right]_i = 0. \tag{4}$$

Note that initial conditions are not satisfied when Ro, $\mathrm{E_v}$, $\mathrm{E_h}$ and Fr are small. Hence we are dealing with a singular-perturbation problem and an asymptotic analysis is necessary to eliminate this singularity. Thus, we introduce the following approximations:

$$\begin{aligned} &\mathrm{Ro} = O(\mathrm{Fr}), \quad \omega = \mathrm{Ro}^2/\mathrm{Fr}^2, \\ &\mathrm{E_h} = \hat{\mathrm{E}}_\mathrm{h}\mathrm{Ro}^2, \quad \mathrm{E_v} = \hat{\mathrm{E}}_\mathrm{v}\mathrm{Ro}^2. \end{aligned} \tag{5}$$

For the asymptotic analysis we assume that the parameters: (St, ω, $\hat{\mathrm{E}}_\mathrm{h}$, $\hat{E}_\mathrm{v}$) are fixed and of order unity.

3. The central equation

We now assume that the parameters Ro and Fr are small and are of the same order (see Equation (5)). The asymptotic expansions of $\mathbf{v}$, w, p, ρ with respect to Ro produces, at the zeroth order:

$$p_0 = p_0(z), \quad \varrho_0 = \varrho_0(z), \quad \mathbf{D}p_0 = 0, \tag{6}$$

$$\mathbf{v}_0 = \frac{\omega}{\varrho_0}\mathbf{k} \times \mathbf{D}p_1, \quad \frac{\mathrm{d}p_0}{\mathrm{d}z} = -\mathrm{Bo}\varrho_0, \tag{7, 8}$$

where the two last equations are the geostrophic and the hydrostatic approximations, respectively. The next order balance is interesting, not only because it causes corrections in the solution, but also because it allows us to follow the slow evolution of the dominant fields. Thus we obtain, to the order of Ro:

$$\varrho_0\left[\mathrm{St}\frac{\partial \mathbf{v}_0}{\partial t}+\mathbf{v}_0\cdot\mathbf{D}\mathbf{v}_0+\beta y\mathbf{k}\times\mathbf{v}_0+\mathbf{k}\times\mathbf{v}_1\right]+\varrho_1\mathbf{k}\times\mathbf{v}_0+\frac{1}{\omega}\mathbf{D}p_2=0$$
$$\frac{\partial p_1}{\partial z}+\mathrm{Bo}\varrho_1=\mathbf{0},\quad \mathbf{D}\cdot\mathbf{v}_1+\frac{\partial w_1}{\partial z}=0,\quad \mathrm{St}\frac{\partial \varrho_1}{\partial t}+\mathbf{v}_0\cdot\mathbf{D}\varrho_1+w_1\frac{\partial \varrho_0}{\partial z}=0. \tag{9a,b,c,d}$$

On using the formula: $\mathbf{a}\times(\mathbf{b}\times\mathbf{c})=(\mathbf{a}\cdot\mathbf{c})\cdot\mathbf{b}-(\mathbf{a}\cdot\mathbf{b})\cdot\mathbf{c}$ and the additional condition $\mathbf{k}\cdot\mathbf{v}_1=0$, we deduce from (9a):

$$\varrho_0\mathbf{v}_1=\varrho_0\left[\mathrm{St}\frac{\partial}{\partial t}(\mathbf{k}\times\mathbf{v}_0)+\mathbf{k}\times(\mathbf{v}_0\cdot\mathbf{D}\mathbf{v}_0)-\beta y\mathbf{v}_0\right]-\varrho_1\mathbf{v}_0+\frac{1}{\omega}\mathbf{k}\times\mathbf{D}p_2 \tag{10}$$

and from (9c) we have:

$$\mathbf{D}\cdot\mathbf{v}_1=-\frac{\partial w_1}{\partial z}.$$

This last equation is then used in (10) to eliminate the second-order pressure variable p_2. Thus, on using (7) we obtain from (10):

$$\varrho_0\frac{\partial w_1}{\partial z}=w\frac{\mathrm{d_h}}{\mathrm{d}z}\mathbf{D}^2p_1+\varrho_0\beta\mathbf{v}_0\cdot\mathbf{j}+\mathbf{v_0}\cdot\mathbf{D}\varrho_1=0. \tag{11}$$

Eliminating ϱ_1 from (9c) and (9d),we obtain an equation for $\mathbf{w}_1$:

$$\mathbf{w}_1=\frac{1}{\mathrm{Bo}}\left(\frac{\mathrm{d}\varrho_0}{\mathrm{d}z}\right)^{-1}\frac{\mathrm{d_h}}{\mathrm{d}z}\left(\frac{\partial p_1}{\partial z}\right). \tag{12}$$

Using (11) and (12), we obtain an equation for the evolution of the perturbation p_1:

$$\frac{\mathrm{d_h}}{\mathrm{dt}}\left[\mathbf{D}^2p_1+\frac{\omega}{\mathrm{Bo}}\left\{\frac{\partial}{\partial z}\left\{-\frac{\varrho_0(z)}{\varrho_0'(z)}(\frac{\partial p_1}{\partial z})\right\}+\frac{\partial p_1}{\partial z}\right\}+\varrho_0(z)\beta\omega y\right]=0, \tag{13}$$

where

$$\frac{\mathrm{d_h}}{\mathrm{dt}}=\mathrm{St}\frac{\partial}{\partial t}+\mathbf{v_0}\cdot\mathbf{D} \tag{14}$$

and

$$\mathbf{D}=\frac{\partial}{\partial x}\mathbf{i}+\frac{\partial}{\partial y}\mathbf{j}.$$

The problem now is reduced to the study of the evolution equation (13) that gives us the pressure perturbation p_1. Thus, the associate boundary conditions are determined while presupposing the existence of two Ekman boundary layers, one at the ocean–atmosphere interface and one at the bottom. However, these Ekman layers are very thin and are dependent on the ways in which the frictional boundaries evolve and on the small parameter $\mathrm{E_v}$. On this subject an analysis has been carried out in [15] and a more detailed one can be found in [14]. In [15] an asymptotic analysis based on singular-perturbation theory is proposed to isolate and to treat separately regions of different physical composition and then match them to each other. Hence, to take into account the smallness of the Ekman layer when $\mathrm{E_v}$ is small, we used the following scales, appropriate for both the surface and bottom-boundary Ekman layers $\xi=(z+1)/\mathrm{Ro}$ for the bottom layer and $\xi=z/\mathrm{Ro}$ for the surface layer. After matching solutions, we could subsequently determine the horizontal and vertical velocities at these boundary layers (the details of this analysis are given in [15]). Using the results of the matching procedure and making an intermediary calculation, we can deduce from (9a) and (12) the following boundary conditions:

$$\frac{\mathrm{d_h}}{\mathrm{dt}}\left(\frac{\partial p_1}{\partial z}\right) = \begin{cases} \Gamma(z)\varkappa(z)\varpi\mathbf{D}^2(\varrho_0^{-1}p_1), & \text{at} \quad z=0 \\ \\ \varkappa(z)\varpi\mathbf{D}^2(\varrho_0^{-1}p_1), & \text{at} \quad z=-1 \end{cases}, \tag{15}$$

where:

$$\Gamma(z) = -1 + \frac{\mu\varrho_0(z)^{1/2}}{\mu\varrho_0(z)^{1/2} + \mu^a\varrho_0^a(z)^{1/2}} < 0$$

with μ being the coefficient of the dynamic viscosity. The superscript 'a' refers to the term 'atmospheric' and designates the signature left by the effects of the atmospheric boundary layer during the matching procedure

$$\varkappa(z) = \left(\frac{\hat{\mathrm{E}}_\mathrm{v}}{2}\right)^{1/2} \frac{\varrho_0'(z)}{\varrho_0(z)^{1/2}}, \quad \varpi = \frac{\mathrm{Bo}}{\omega} = O(1)$$

In the following, we propose a solution for Equation (13) with the boundary conditions (15). The main goal of this study is to show that the vertical structure of the pressure perturbation p_1 depends on the density gradient and, therefore, on stratification. Hence, because of the anisotropy between large horizontal scales (∼100 km) and vertical scales (∼4 km) of the phenomena being considered in this paper, it is necessary to differentiate between the dynamics involved in large-scale movements in either direction. In the horizontal plane (*i.e.* in the x- and y-directions), large-scale movements can be regarded as isotropic. In such circumstances, there are certain simplifications that can be made; namely, the technique of separating variables in order to express the solution as a sum of normal modes. This method provides a good description of the vertical structure of the solution in the case of a continuously stratified ocean. In restricting our attention to the vertical structure we therefore consider plane waves of the form:

$$p_1(x, y, z, t) = P(z)\exp\{\mathrm{i}(kx + ly - \sigma t)\} \tag{16}$$

Depending on the physical problem being studied, other wave forms can be used. For example, to study the vertical concentration of internal waves on a pycnocline level in which horizontal inhomogeneities of density or current are also present, Badulin *et al.* [3] proposed a solution of the form:

$$p(x, y, z, t) = p(\varepsilon y, z)\exp\left\{\mathrm{i}\left(kx + \int l(\varepsilon y)\,\mathrm{d}y - \sigma t\right)\right\}$$

where ε is a small parameter equal to the ratio of the typical wavelength λ_0 and the characteristic scale of the horizontal inhomogeneity D.

Substituting the equation (16) in Equations (13) and (15), we obtain:

$$\mathrm{H_s}(z)\frac{\mathrm{d}^2P(z)}{\mathrm{d}^2z} + \left(1 + \mathrm{H_s'}(z)\right)\frac{\mathrm{d}P(z)}{\mathrm{d}z} - \lambda P(z) = 0, \tag{17}$$

where $\lambda = K_h^2 + k\beta/\sigma$ with $K_h^2 = k^2 + l^2 \cdot K_h^2$ is the horizontal wave number, where k and l are the wave numbers in the x- and y-directions and where σ is the frequency of the free harmonic waves.

The associated boundary conditions at the top and at the bottom are, respectively:

$$\begin{cases} (-\sigma \mathrm{St} + \mathbf{v_0} \cdot \boldsymbol{\nabla}) \frac{\mathrm{d}P(0)}{\mathrm{d}z} - \alpha_2 P(0) = 0 \\ \\ (-\sigma \mathrm{St} + \mathbf{v_0} \cdot \boldsymbol{\nabla}) \frac{\mathrm{d}P(-1)}{\mathrm{d}z} - \alpha_1 P(-1) = 0 \end{cases}, \tag{18}$$

where St designates the Strouhal number, $\mathbf{v_0}$ is given by (7), i is the imaginary unit and $\boldsymbol{\nabla}$ is the vector:

$$\boldsymbol{\nabla} = k\mathbf{i} + l\mathbf{j} \tag{19}$$

with $\mathbf{i}$ and $\mathbf{j}$ being the unit vectors. The parameters α_1 and α_2 are given by:

$$\alpha_2 = -\mathrm{i}K_h^2 \Gamma(0) \hat{\mathrm{E}}_{\mathrm{v}}^{1/2} / \left(2H_s^{-1} \varrho_0^{1/2}(0)\right), \quad \alpha_1 = -\mathrm{i}K_h^2 \hat{\mathrm{E}}_{\mathrm{v}}^{1/2} / \left(2H_s^{-1} \varrho_0^{1/2}(-1)\right), \tag{20}$$

where

$$H_s^{-1}(z) = -\frac{\varrho_0'(z)}{\varrho_0(z)} = \frac{N_m^2(z)}{g}$$

with $H(z)$ designating the vertical density scale, and $N_m^2(z)$ being the square of the Brunt–Väisälä frequency.

The problem derived in (17), of which the boundary conditions are formulated in (18) constitutes an eigenvalues problem whose solution gives us the vertical distribution of the $P(z)$ pressure perturbation. The λ scalars are the eigenvalues in this problem.

4. Analysis of modal solutions for continuous stratification

In this section, we will focus on the Sturm–Liouville problem (17–18), while taking expressions of the density profile into account. Our aim is to obtain a sequence of eigenvalues λ_n (or σ_n) and to estimate the corresponding eigenfunctions $P_n(z)$. The complexity of this problem is caused by the presence of eigenvalues in the boundary conditions, so that the set of Equations (17) and (18) are rendered non-orthogonal. In order to overcome this difficulty and to construct an asymptotic solution, we adopt the following new approximation: $\mathrm{St} = \varepsilon \ll 1$, where St is the Strouhal parameter. This approximation means that we are dealing with a quasi-stationary flow. Hence, for small ε, we seek an asymptotic expansion of the variables in powers of ε in the form: $\sum_{i=0}^{\infty} \varepsilon^i f^i$, where f can denote any of P, σ and λ.

At the zeroth order of ε, Equation (17) yields

$$\frac{\mathrm{d}}{\mathrm{d}z}\left(\frac{1}{\rho_0'(z)} \frac{\mathrm{d}P_1(z)}{\mathrm{d}z}\right) + \frac{\lambda_1}{\rho_0(z)} P_1(z) = 0 \tag{21}$$

with the boundary conditions:

$$-(\mathbf{v_0} \cdot \boldsymbol{\nabla}) \frac{\mathrm{d}P_1}{\mathrm{d}z} + \alpha_2 P_1 = 0 \quad \text{at} \quad z = 0, \quad -(\mathbf{v_0} \cdot \boldsymbol{\nabla}) \frac{\mathrm{d}P_1}{\mathrm{d}z} + \alpha_1 P_1 = 0 \quad \text{at} \quad z = -1. \tag{22}$$

It has been shown (Bois *et al.* [16], Ouahsine [17]) that, for the constant stratification case, when the density profile has an exponential form: $\rho_0(z) = \rho_{00} \exp(-\mathrm{N}_{\mathrm{m}}^2 z)$, which means that a solution of the eigenvalues problem has been identified which describes stable periodic Rossby waves. When the friction effects resulting from the viscosity appear in the equations of motion (by using the Ekman number to establish the boundary conditions), the waves lose their

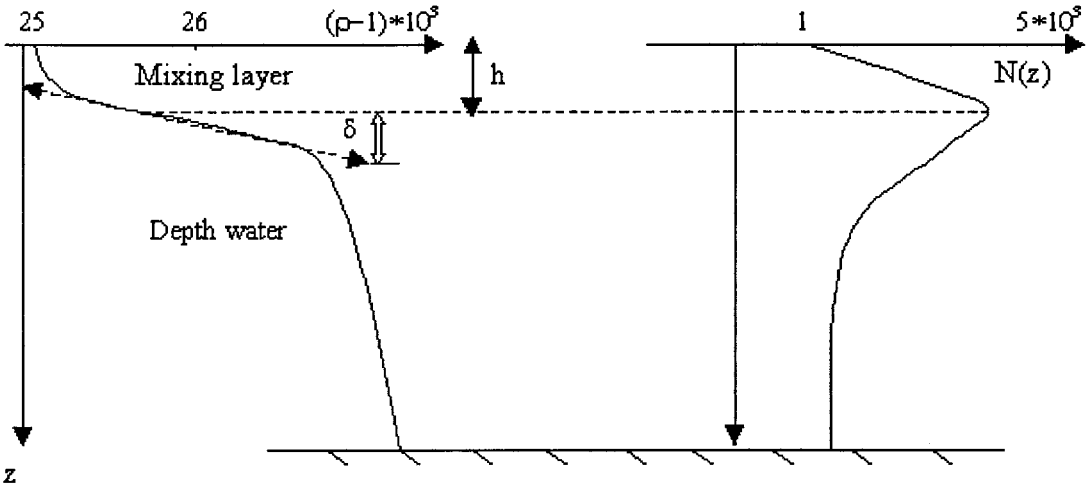

Figure 1. A schematic representation of density distribution in the ocean, and the corresponding Brunt-Väisälä frequency N(z).

periodic character and their energy dissipates. This leads us to conclude that classical baroclinic Rossby waves propagate vertically and remain stable when the stratification is constant. Laboratory observations [18] have confirmed these results, and no evidence of frontogenesis or any internal instabilities was found. However, this vertical stability does not occur in cases of nonuniform stratification. To illustrate this point, we consider an example of a density distribution in tanh form, a form that may qualitatively approximate a typical oceanic profile (see Figure 1):

$$\rho_0(z) = \rho_{00}\left[1 - \mathrm{N}_\mathrm{m}^2 \tanh\left(\frac{z+h}{\delta}\right)\right], \tag{23}$$

where $\mathrm{N}_\mathrm{m}^2 \ll 1$ and ρ_{00} are constants. Thus, the density scale height reads:

$$H_s^{-1}(z) = \frac{\mathrm{N}_\mathrm{m}^2}{\delta \cosh\left(\dfrac{z+h}{\delta}\right)} + O(\mathrm{N}_\mathrm{m}^4), \tag{24}$$

where $0 < \delta < 1$ is the varying stratification parameter and g is the gravitational acceleration. Following a classical procedure (see for example [19]), the equations of motion (17–20) may be transformed into a suitable form by the introduction in place of z of a new variable ξ defined as follows:

$$\xi = \frac{1}{J}\int_{-1}^{z}\left(-\frac{\rho_0(z)}{\rho_0'(z)}\right)^{1/2} \mathrm{d}t, \tag{25}$$

where

$$J = \int_{-1}^{0}\left(-\frac{\rho_0(z)}{\rho_0'(z)}\right)^{1/2} \mathrm{d}t$$

and instead of the function $P_1(z)$ we introduce a new function:

$$X(\xi) = P_1(z)\left(\frac{-1}{\rho_0(z)\rho_0'(z)}\right)^{1/4}. \tag{26}$$

This yields the following modified Sturm–Liouville problem:

$$\begin{aligned} &\frac{\mathrm{d}^2X(\xi)}{\mathrm{d}\xi^2} - (\eta_1^2 + V(\xi,\delta))X(\xi) = 0 \\ &\frac{\mathrm{d}X(1)}{\mathrm{d}\xi} - aX(1) = 0 \quad \text{and} \quad \frac{\mathrm{d}X(0)}{\mathrm{d}\xi} - bX(0) = 0, \end{aligned} \tag{27}$$

where

$$\eta_1^2 = \lambda_1 J^2, \quad V(\xi,\delta) = \frac{1}{16}\left[\frac{5\rho_0'^2(\xi)}{\rho_0^2(\xi)} - \frac{2\rho_0''(\xi)}{\rho_0(\xi)} + \frac{5\rho_0''^2(\xi)}{\rho_0'^2(\xi)} - \frac{4\rho_0'''(\xi)}{\rho_0'(\xi)}\right].$$

This last expression may be written more clearly:

$$V(\xi,\delta) = \frac{1}{2\delta^2}\left[1 - \frac{\tanh^2\left(\frac{\xi-1+h}{\delta}\right)}{2} - \frac{\mathrm{N}_\mathrm{m}^2}{2}\frac{\sinh\left(\frac{\xi-1+h}{\delta}\right)}{\cosh^3\left(\frac{\xi-1+h}{\delta}\right)} + \frac{5}{8}\frac{\mathrm{N}_\mathrm{m}^4}{\cosh^4\left(\frac{\xi-1+h}{\delta}\right)}\right] \tag{28}$$

and

$$\begin{aligned} a &= \frac{\alpha_2 H_s(0) J}{\mathbf{v_0}\cdot\boldsymbol{\nabla}} - \frac{1}{4}\left[\frac{\rho_0'(\xi)}{\rho_0(\xi)} + \frac{\rho_0''(\xi)}{\rho_0'(\xi)}\right]_{\xi=1}, \\ b &= \frac{\alpha_1 H_s(-1) J}{\mathbf{v_0}\cdot\boldsymbol{\nabla}} - \frac{1}{4}\left[\frac{\rho_0'(\xi)}{\rho_0(\xi)} + \frac{\rho_0''(\xi)}{\rho_0'(\xi)}\right]_{\xi=0}, \end{aligned} \tag{29}$$

where $\mathbf{v_0}$ is given by (7) and $\boldsymbol{\nabla}$ by (19).

The set of Equations (27) constitute a homogeneous boundary-value problem, for which we need to find nontrivial solutions (eigenfunctions) and to determine the corresponding values of the separation parameter (eigenvalues). In the following analysis we consider only the case where η_1^2 is negative: $\eta_1^2 = -\mu_1^2$. Since η_1^2 is negative, we have:

$$\lambda_1 = k^2 + l^2 + \frac{k\beta}{\sigma_1} < 0. \tag{30}$$

Using a classical mathematical argument (see [20]), we may give eigenfunctions of the problem (27) as:

$$X(\xi) = C_1\ \cos(\mu_1\xi) + C_2\ \sin(\mu_1\xi) + \frac{1}{\mu_1}\int_0^\xi [V(t,\delta)\ \sin(\mu_1(\xi-t))X(t)]\,\mathrm{d}t, \tag{31}$$

where C_1 and C_2 are constants. From the first boundary condition at $\xi = 0$ we determine the coefficient C_2, so that (31) reads:

$$X(\xi) = C_1\left(\cos(\mu_1\xi) + \frac{b}{\mu_1}\ \sin(\mu_1\xi)\right) + \frac{1}{\mu_1}\int_0^\xi [V(t,\delta)\ \sin(\mu_1(\xi-t))X(t)]\,\mathrm{d}t. \tag{32}$$

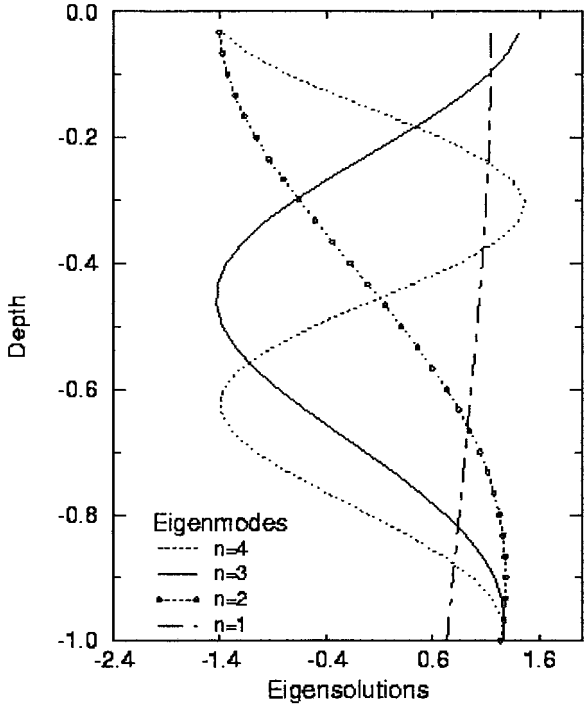

Figure 2. First four baroclinic modes for eigenfunctions when the value of parameter $\delta = 1$.

From the second condition at $\xi = 0$ we then deduce the following dispersion-wave equation:

$$\text{tang}\,(\mu_1) = \frac{C_1(b-a) + \int_0^1 |V(t,\delta)| \left[\cos(\mu_1 t) + \dfrac{a}{\mu_1}\sin(\mu_1 t)\right] X(t)\,\mathrm{d}t}{C_1(\mu_1 + \dfrac{a}{\mu_1}) - \int_0^1 |V(t,\delta)| \left[\sin(\mu_1 t) - \dfrac{a}{\mu_1}\sin(\mu_1 t)\right] X(t)\,\mathrm{d}t}. \tag{33}$$

The roots of this equation form a discrete spectrum ($\mu_{1n}, n = 1, 2, \dots$). Thus, if μ_{1n} are sufficiently large, Equation (33) can be approximated by (see [17]):

$$\mu_{1n} \cong n\pi + \frac{(b-a) + \frac{1}{2}\int_0^1 |V(t,\delta)|\,\mathrm{d}t}{n\pi} + O\left(\frac{1}{n^2}\right), \quad (n = 1, 2, \dots). \tag{34}$$

The first four baroclinic eigenfunctions are plotted in Figure 2. However, the Sturm–Liouville fundamental existence theorem ([20], pp. 266–278) indicates that, if the coefficients C_1 and C_2 of (31) are bounded and continuous, then there exists a fixed number $M = \text{Sup}_\xi |X(\xi)|$ such that:

$$|X(\xi)| \leq M. \tag{35}$$

It follows from the Schwarz inequalities and from (32) and (35) that, when $\mu_1 \neq 0$, we have:

$$|X(\xi)| \leq |C_1| \left(1 + \frac{b^2}{\mu_1^2}\right)^{1/2} + \frac{M}{\mu_1} \int_0^1 |V(t, \delta)| \, \mathrm{d}t. \tag{36}$$

Note that one can find a positive δ_0 for which there is an associated positive upper bound any M_0 independent of the parameter μ_1. In the resulting range, $\delta_0 \leq \delta < 1$, we obtain:

$$M \leq |C_1| \left(1 + \frac{b^2}{\mu_1^2}\right)^{1/2} \Bigg/ \left\{1 - \frac{1}{\mu_1} \int_0^1 |V(t, \delta)| \, \mathrm{d}t\right\} \leq M_0. \tag{37}$$

From this last inequality, the variation of the varying stratification parameter δ implies the variation of the potential function $V(t, \delta)$. Thus, in the range $0 < \delta < \delta_0$, the upper bound M may have negative values or may be excessively large if the denominator in (37) is reduced to zero. In any case, a critical state may be reached when μ_1 asymptotically approaches a limit value, namely:

$$\mu_1^c \cong \int_0^1 |V(t, \delta_{\mathrm{cri}})| \, \mathrm{d}t. \tag{38}$$

In the vicinity of this limit value μ_1^c, the upper bound M_0 gets sufficiently large to cause an enlargement of the solution amplitudes. This means that, in the range $0 < \delta < \delta_0$, a significant increase in wave amplitudes is observed when the waves approach the upper layers on the density gradient. This amplification is accompanied by a transformation of the vertical structure of internal wave-modes (Figure 3) and renders the vertical wave propagation unstable. When the critical value δ_{cri} is attained, increases in solution amplitude can only be limited by wave-breaking and viscous dissipation. The same features were also observed in experiments ([10], [18])

In this study, we have already discussed a linear analysis to derive the growth rate of the finite-amplitude waves. The instability was then interpreted as a criterion in which the wave amplitudes grow, in inverse proportion to the parameter of varying stratification δ, until the limit resulting in wave breaking is attained. When the wave amplitude grows, to such a level that δ drops below the critical value, the perturbations can grow exponentially to the point that the primary wave amplitude exceeds a limit value of tolerances. The stability process described here implies that, initially, the density distribution of the fluid on either side of the turbulent region is assumed to be homogeneous. When an appreciable density difference between the turbulent and non-turbulent regions develops, new effects occur. A thin pycnocline or thermocline layer develops, in which the ambient fluid is initially statically stable (*i.e.* $\partial\rho_0/\partial z < 0$). However, if there is sufficient shear or wave energy coming from the breaking or from large-amplitude internal-waves, dynamical instability occurs which gives rise to vortical formations (rolls or billows). When the breaking mechanism occurs, a linear analysis is no longer valid and a nonlinear analysis is necessary in order to account for the low-frequency waves. In the case of high turbulent activity, for example when the density difference at the interface is significant and the interface is very thin, these vortical structures can be mobile and give rise to fronts. Several experimental and theoretical studies have been carried out on this subject. Laget and Dias [21], for example, have conducted a numerical study on the propagation of interfacial solitary waves. They have shown that there are capillary gravity waves bifurcating from a basic uniform flow in the form of wave packets that are known to

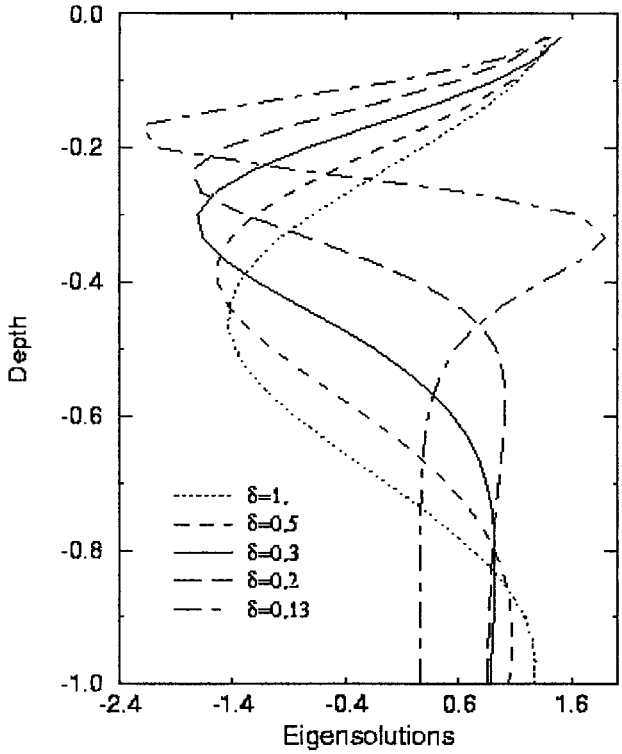

Figure 3. Amplitude variations of eigenfunctions in terms of the varying stratification parameter δ and for the eigenmode $n = 3$.

exist for small density ratios. In the case of a rigid-lid configuration, these waves exist also for larger density ratios, but only at finite amplitude, and bifurcate at a critical value of the fluids velocity c given by

$$c^2 = gh_1 \frac{H(1-R)}{H+R},$$

where h_1 denotes the depth of the lower layer, H the ratio of fluids depths h_2/h_1, R the ratio of densities

$$\frac{\rho_2}{\rho_1}(\rho_1 > \rho_2)$$

and g the acceleration due to gravity. However, when the Weber number: $W = \sigma/[\rho_1(h_1 + h_2)c^2]$ where σ is the coefficient of interfacial tension, is non-zero and less than a critical value $W^* = \frac{1}{3}(1 + RH)/(1 + H)$, solitary waves are generated [21]. The authors performed a numerical analysis of the case when $W > W^*$ and showed that solitary waves in the form of wave packets exist, even for larger density ratio R but only at finite amplitude. These waves are in elevation if $H^2 - R < 0$ and in depression if $H^2 - R > 0$. Therefore, when $H^2 \simeq R$, there are gravity-wave fronts. In this case, solitary waves bifurcate from a train of infinitesimal periodic waves in the form of wave packets. As $F = 1/(1 + R^{1/2})$ increases with a fixed $H_1 = h_1/(h_2 + h_1)$, the amplitude of these solitary waves increases and the wave broadens. As F reaches a critical value, the broadening becomes infinite. In their experimental and analytical investigations, Pawlak and Armi [11] studied the effect of the density offset where the density profile is defined by (see Figure 4):

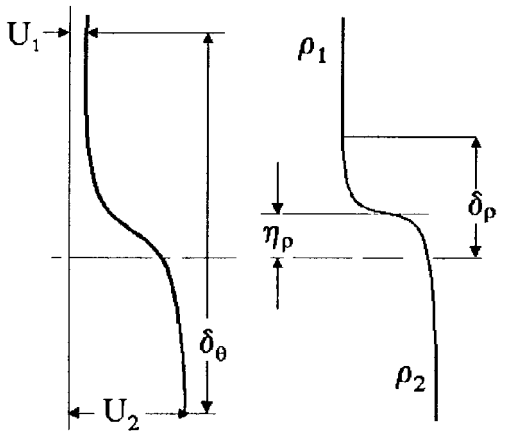

Figure 4. Velocity and density profiles, used by Pawlak and Armi [11].

$$\rho = \rho_0 \exp\left(-\frac{\rho_2 - \rho_1}{\rho_0} \tanh\left(R(\hat{y} - \eta_\rho)\right)\right),$$

where $\rho_0 = \frac{1}{2}(\rho_2 + \rho_1)$, η_ρ is the offset of the density interface from the velocity interface (η_ρ is equivalent to the parameter δ in our study), $R = \delta_\theta/\delta_\rho$ and $\hat{y} = y/2\delta_\theta$ is the vertical coordinate. They found two relevant solution types. The fastest growing mode, called mode A, and a slower growing solution called mode B. The faster growing mode A shows significant displacement of its centre of rotation towards the low-momentum side and is characterized by a high spatial growth rate with an increase in the most unstable wave numbers for $\eta_\rho = 0$. A positive density offset results in a decrease in growth rate along with an increase in the most unstable wave numbers. Mode B, undergoes an increase in growth rate and a decrease in the fastest growing wave numbers for a positive η_ρ. A negative η_ρ results in an increase in growth rate and a decrease of the most unstable wave numbers for mode A with the opposite effect being observed for mode B [11].

5. Eigensolutions with discontinuous gradients of density

In this section we deal with the set of equations given in (17–18) and seek to obtain eigenvalues when the stratification parameter δ is very small. For simplicity we assume that $\hat{E}_v \ll 1$. In most problems of geophysical interest the parameter $\hat{E}_v$ is generally small for mid-latitude ocean flows (see [22], pp. 102–117). If the horizontal scale L is about 10^3 km, the vertical scale H is about 5 km and the horizontal velocity U is about 1 m/s, with the kinematic viscosity varying between 5×10^{-3} and 5×10^{-2} m^2/s, the depth of the Ekman layer is of the order of 6 m to 20 m [22]. The corresponding values of the parameter $\hat{E}_v$ are small and vary from $2{\cdot}67 \times 10^{-2}$ to $2{\cdot}67 \times 10^{-1}$. Thus, the Ekman layer occupies only a small fraction of the fluid depth. Yet, from the preceding section, the analysis of the vertical structure of the perturbation pressure explicitly exploits the thinness of this layer and does not reveal any particular problem due to the presence or absence of the parameter $\hat{E}_v$ in the boundary conditions.

Hence on the basis of (17–18) and accounting for the density profile given by (23), we can formulate the following equation:

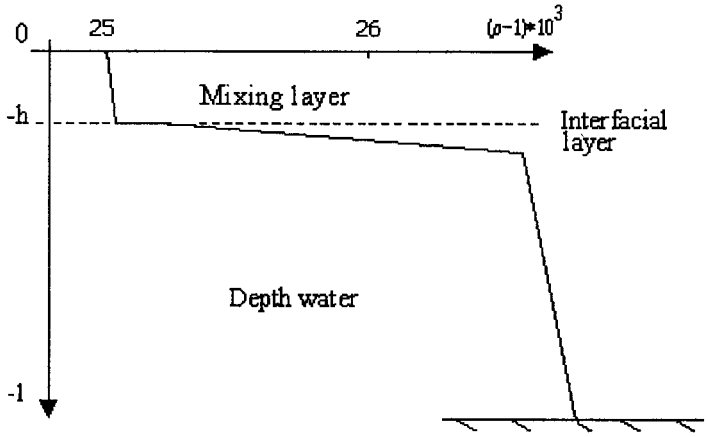

Figure 5. Three-layer schematic representation of density in the case $\delta \ll 1$.

$$\frac{\mathrm{d}^2 P_1(z)}{\mathrm{d}^2 z} + \frac{2}{\delta}\ \tanh\left(\frac{z+h}{\delta}\right)\frac{\mathrm{d}P_1(z)}{\mathrm{d}z} - \frac{\lambda \mathrm{N}_\mathrm{m}^2}{\delta\ \cosh^2\left(\frac{z+h}{\delta}\right)}\Bigg(1+ \\ +\mathrm{N}_\mathrm{m}^2\ \tanh\left(\frac{z+h}{\delta}\right)\Bigg)P_1(z) = 0, \tag{39}$$

where $\delta \ll 1$ and $\mathrm{N}_\mathrm{m}^2 \ll 1$. We subsequently suppose that

$$\frac{\mathrm{N}_\mathrm{m}^2}{\delta} = O(1) \tag{40}$$

and make the following transformation

$$P_1(z) = \Phi(\xi)\ \cosh^m\left(\frac{z+h}{\delta}\right), \tag{41}$$

where m is a factor yet to be determined and ξ is given by:

$$\xi = \cosh^2\left(\frac{z+h}{\delta}\right). \tag{42}$$

As $\delta \to 0$, there are two cases of interest (Figure 5):

(i) when $z \neq -h$ (then $\xi \to \infty$), $\quad (ii)$ when $z = -h$ (then $\xi \to 1$)

This leads us to formulate two differently structured solutions (Figure 5): one solution valid near the surface discontinuity (*i.e.* when $z = -h$), and another solution valid in two regions on either side of the frontier designated by $z \neq -h$. From (41) and (42), the equation that solves Φ and the associate boundary conditions, reads:

$$\xi(\xi-1)\Phi''(\xi) + \left((m+2)\xi - \left(m+\frac{3}{2}\right)\right)\Phi'(\xi) + \frac{m^2}{4}\Phi(\xi) = 0, \tag{43}$$

$$\Phi'_{(\xi\to\infty)}(\xi) = 0, \quad \Phi'_{(\xi\to 1)}(\xi) = 0. \tag{44}$$

Equation (43) is a hypergeometric differential equation of which $\xi = 1$ and $\xi \to \infty$ are the singular points and where m is related to the eigenvalues by

$$m(m-1) = -\lambda \mathrm{N}_{\mathrm{m}}^2 \delta. \tag{45}$$

When $\xi \to \infty$, the analytical solution satisfying the condition $\Phi'(\xi) = 0$ is given by

$$P_{1\infty} = A\left[\xi^{-\frac{1+\ell}{2}} F\left(\frac{m+1+\ell}{2}, \frac{-m+\ell}{2}; 1+\ell, \xi^{-1}\right)\right], \tag{46}$$

where F is the hypergeometric function of which the development according to the Gauss series can be written

$$F(a,b;c,x) = \sum_{n=0}^{N} \frac{(a)_n (b)_n}{(c)_n} \frac{x^n}{n!}. \tag{47}$$

In (46), it was posited that

$$\ell = \sqrt{2m+1}$$

and A is an arbitrary constant.

At the interface layer, *i.e.* $z = -h$, the solution takes the following analytical form:

$$\begin{aligned} P_{11} = \; & C\left[\xi^{\frac{m}{2}} F\left(\frac{m+1+\ell}{2}, \frac{m+1-\ell}{2}; \frac{1}{2}, 1-\xi\right)\right] + \\ & D\left[\xi^{\frac{m}{2}} (1-\xi)^{1/2} F\left(\frac{m+2-\ell}{2}, \frac{m+2+\ell}{2}; \frac{3}{2}, 1-\xi\right)\right], \end{aligned} \tag{48}$$

where the constants C and D, undetermined in (48), are to be obtained by matching solutions (46) and (48). This matching must express the continuity of the solution when $\xi = 1$, a requirement met by using analytical continuation to transform (46) into two independent solutions in the neighborhood of $\xi = 1$ [23]. Hence,

$$\begin{aligned} P_{1\infty} = \; & \alpha_{1\infty}\left[A\xi^{\frac{m}{2}} F\left(\frac{m+1+\ell}{2}, \frac{m+1-\ell}{2}; \frac{1}{2}, 1-\xi\right)\right] + \\ & \alpha_{2\infty}\left[A\xi^{-\frac{(m+1)}{2}} (\xi-1)^{1/2} F\left(\frac{-m+1+\ell}{2}, \frac{-m+1-\ell}{2}; \frac{3}{2}, 1-\xi\right)\right], \end{aligned} \tag{49}$$

with

$$\alpha_{1\infty} = \frac{\Gamma((1+\ell)/2)\Gamma(\frac{1}{2})}{\Gamma((-m+1+\ell)/2)\Gamma((m+2+\ell)/2)}, \tag{50}$$

$$\alpha_{2\infty} = \frac{\Gamma((1+\ell)/2)\Gamma(-\frac{1}{2})}{\Gamma((-m+1+\ell)/2)\Gamma((-m+\ell)/2)}, \tag{51}$$

where Γ is the gamma function. The solutions given in (48) and (49) can be matched only if

$$\alpha_{2\infty} = 0. \tag{52}$$

Since the gamma function satisfies the property:

$$\frac{1}{\Gamma(-n)} = 0 \tag{53}$$

for $n \geq 0$, (51) and (53) lead to:

$$m + 1 + \sqrt{2m + 1} = -2n. \tag{54}$$

From this last equation and (45) we deduce the problem eigenvalues:

$$\lambda_n = \frac{4}{\delta \mathrm{N}_\mathrm{m}^2}\{n(1 - 2n) + \mathrm{i}(4n + 1)n^{1/2}\}, \quad (n = 0, 1, 2, \dots). \tag{55}$$

The corresponding eigenfunctions read:

$$P_{1n}(\xi) = \alpha_{1n} A \xi^{m_n/2} F(-n, -n - \sqrt{2m_n + 1}; \tfrac{1}{2}, 1 - \xi), \tag{56}$$

where m_n is the root of (54) associated with n. To have the roots λ_n corresponding to (55), m_n must satisfy the following relationship:

$$m_n = -2n + 2\mathrm{i}n^{1/2}. \tag{57}$$

In order to fully exploit the solution (55) to study the stability of the eigensolutions) it is now necessary to ask if the σ frequency introduced in (16) has an imaginary positive or negative part. In (55), we see that λ is complex; it may either be written in terms of its real and imaginary components ($\lambda = \lambda_r + \mathrm{i}\lambda_i$), while also taking into account the relationship (30) between λ and σ, which is given by

$$\lambda = K_h^2 + \frac{k\beta}{\sigma}$$

or σ may written on the basis of (55) as $\sigma = \sigma_r + \mathrm{i}\sigma_i$, with:

$$(\sigma_r)_n = \frac{-k\beta\{|(\lambda_r)_n| + K_h^2\}}{[(\lambda_r)_n - K_h^2]^2 + (\lambda_i)_n^2}, \quad (n = 0, 1, 2, \dots), \tag{58}$$

$$(\sigma_i)_n = \frac{-k\beta|(\lambda_i)_n|}{[(\lambda_r)_n - K_h^2]^2 + (\lambda_i)_n^2}, \quad (n = 0, 1, 2, \dots), \tag{59}$$

These last equations are the dispersion relations for Rossby waves.

Since the wave number k and the β-number are positive, it follows from the analysis of Equation (59) that $(\sigma_i)_n$ is always negative. Hence, over very long periods of time, the growth rate $\exp[(\sigma_i)_n t]$ reduces to zero when $(\sigma_i)_n < 0$. In accordance with (16), we deduce that the solutions are stable and are decreasing, as time becomes large.

6. Conclusions

The mathematical model of long ocean waves presented in this paper allows us to study the behavior of internal waves in a fluid with variable stratification by using the Boussinesq approximation. In order to simulate large-scale wave motions, we have formulated the dimensionless Navier-Stokes equations, into which we have introduced the Rossby number Ro, the Froude number Fr, and both the vertical and horizontal Ekman numbers: $\mathrm{E_v}$ and $\mathrm{E_h}$ respectively. These parameters, when they are small, permit us to reduce the problem to one involving a singular perturbation. Successive estimations of the velocity field and the pressure perturbation result in the formulation of a single evolution equation for the pressure

perturbation. The problem is then reduced to the problem of Sturm–Liouville eigenvalues. A few principal properties of the frequencies and modal structures of the eigenmodes are then exhibited. It was shown that these solutions are stable and involved in periodic movement when the stratification is constant. If the density stratification varies with depth, the nature of the vertical structure of the pressure perturbation seems to depend on the varying stratification parameter denoted by δ. The results of the model indicated that a significant growth of the solution amplitude develops as δ approaches a critical value δ_{cri}, producing interfacial waves, which may lead to the formation of frontogenesis. This process showed that, the sharper the interface is, the more unstable the vertical structure of the waves will be, and therefore the growth of the wave amplitude can only be restricted by wave-breaking and by viscous dissipation.

When the varying stratification parameter δ was sufficiently small ($\delta < \delta_{\text{cri}}$) an asymptotic analysis of the problem was proposed. Using a three-layer discontinuous gradient model, this analysis consists in specifying one solution within the interfacial layer and two solutions on either side of this layer. After implementing the appropriate interfacial conditions to ensure proper matching, a generally matched solution was produced, even when there were very small values of the parameter δ.

References

1. J.L. McGrath H.J.S. Fernando and J.C.R. Hunt, Turbulence, waves and mixing at shear-free density interfaces, Part 2 Laboratory experiments. *J. Fluid. Mech.* 347 (1997) 23–61.
2. P.A Bois, Asymptotic aspects for the Boussinesq approximation for gases and liquids. *J. Geophys. Astrophys. Fluid Dyn.* 58 (1991) 4–5.
3. S.I. Badulin V.I. Shrira and L.S.H Tsimring, The trapping and vertical focusing of internal waves in a pycnocline due to the horizontal inhomogeneties of density and currents. *J. Fluid. Mech.* 158 (1985) 19–18.
4. E.J. Hopfinger and P.F. Linden, Formation of thermoclines in zero-mean shear turbulence subjected to a stabilizing buoyancy flux. *J. Fluid Mech.* 114 (1982) 157–173.
5. H.J.S. Fernando, Migration of density interfaces subjected to differential turbulent mixing. *J. Geophys. Astrophys. Fluid Dyn.* 78 (1995) 1–20.
6. I.A. Hannoun H.J.S. Fernando and E.J. List, Turbulence structure near a sharp density interface. *J. Fluid Mech.* 189 (1988) 189–209.
7. P.G. Drazin W. H. Reid, Hydrodynamic Stability. Cambridge University press (1981) 525 pp.
8. J.S. Turner, Buoyancy Effects in Fluids. Cambridge University Press (1973) 367 pp.
9. R.E. Davis and A. Acrivos, The stability of oscillatory internal waves. *J. Fluid Mech.* 30 (1967) 723–736.
10. A.P. Stamp and M. Jacka, Deep water internal solitary waves. *J. Fluid. Mech.* 305 (1995) 347–871.
11. G. Pawlak and L. Armi, Vortex dynamics in spatially accelerating shear layer. *J. Fluid. Mech.* 376 (1998) 347–871.
12. J. Grue A. Jensen P.O. Rusas and J.K. Sveen, Properties of large-amplitude internal waves. *J. Fluid. Mech.* 380 (1999) 257–278.
13. T.B. Benjamin, Internal waves of finite amplitude and permanent form. *J. Fluid. Mech.* 25 (1966) 25–78.
14. J. Pedlosky, Geophysical Fluid Dynamics. Second Edition, Heidelberg: Springer Verlag (1987) 710 pp.
15. S. Godts, Un modèle asymptotique de l'interface océan-atmosphère dans l'étude de l'évolution des courants océaniques. *J. of Theor. Applied Mech.* 7 suppl. 2 (1988) 131–144.
16. P.A Bois S. Godts and A. Ouahsine, Amortissement visqueux des ondes de Rossby dans les courants océaniques par couches de fond et d'interface. *C.R. Acad. Sci. Paris* 312 série II (1991) 435–439.
17. A. Ouahsine, Vertical structure and stability in a mathematical model of the ocean internal waves. *Int. J. Eng. Sci.* 34 (1996) 1311–1326.
18. J.E. Simpson and P.F. Linden, Frontogenesis in a fluid with horizontal density gradients. *J. Fluid. Mech.* 202 (1989) 1–16.
19. P.M. Morse and H. Feshbach, Methods of Theoretical Physics. New York: McGraw-Hill Book Company (1954) 1978 pp.

20. E.L. Ince, *Ordinary differential equations.* New York: Dover (1956) 558 pp.
21. O. Laget and F. Dias, Numerical computation of capillary-gravity interfacial solitary waves. *J. Fluid. Mech.* 349 (1997) 221–251.
22. E.B. Kraus, *Modelling and prediction of the upper layers of the ocean.* Oxford: Pergamon Press (1975) 325 pp.
23. M. Abramowitz and I. Stegun, *Handbook of Mathematical Functions.* New York: Dover publications (1965) 1046 pp.